Am J Physiol Heart Circ Physiol 292: H483–H495, 2007.
First published September 8, 2006; doi:10.1152/ajpheart.00632.2006.

Autocrine/paracrine pattern of superoxide production through NAD(P)H oxidase in coronary arterial myocytes

Guo Zhang,[1,3] Fan Zhang,[1] Rachel Muh,[1] Fan Yi,[1] Karel Chalupsky,[2] Hua Cai,[2] and Pin-Lan Li[1]

[1]*Department of Pharmacology and Toxicology, Medical College of Virginia, Virginia Commonwealth University, Richmond, Virginia;* [2]*Section of Cardiology, Department of Medicine, Division of Biological Sciences and Pritzker School of Medicine, University of Chicago, Chicago, Illinois;* [3] *Research Center of Experimental Medicine, Guangxi Autonomous Region People's Hospital, Nanning, Guangxi, People's Republic of China*

Submitted 14 June 2006; accepted in final form 31 August 2006

Zhang G, Zhang F, Muh R, Yi F, Chalupsky K, Cai H, Li P-L. Autocrine/paracrine pattern of superoxide production through NAD(P)H oxidase in coronary arterial myocytes. *Am J Physiol Heart Circ Physiol* 292: H483–H495, 2007. First published September 8, 2006; doi:10.1152/ajpheart.00632.2006.—The present study tested the hypothesis that membrane-bound NAD(P)H oxidase in coronary arterial myocytes (CAMs) is capable of producing superoxide ($O_2^{\bullet-}$) toward extracellular space to exert an autocrine- or paracrine-like action in these cells. Using a high-speed wavelength-switching fluorescent microscopic imaging technique, we simultaneously monitored the binding of dihydroethidium-oxidizing product to exogenous salmon testes DNA trapped outside CAMs and to nuclear DNA as indicators of extra- and intracellular $O_2^{\bullet-}$ production. It was found that a muscarinic agonist oxotremorine (OXO; 80 μM) increased $O_2^{\bullet-}$ levels more rapidly outside than inside CAMs. In the presence of superoxide dismutase (500 U/ml) plus catalase (400 U/ml) and NAD(P)H oxidase inhibitor diphenylene iodonium (50 μM) or apocynin (100 μM), these increases in extra- and intracellular $O_2^{\bullet-}$ levels were substantially abolished or attenuated. The $O_2^{\bullet-}$ increase outside CAMs was also confirmed by detecting oxidation of nitro blue tetrazolium and confocal microscopic localization of Matrigel-trapped OxyBURST H_2HFF Green BSA staining around these cells. By electron spin resonance spectrometry, the extracellular accumulation of $O_2^{\bullet-}$ was demonstrated as a superoxide dismutase-sensitive component outside CAMs. Furthermore, RNA interference of NAD(P)H oxidase subunits Nox1 or p47 markedly blocked OXO-induced increases in both extra- and intracellular $O_2^{\bullet-}$ levels, whereas small inhibitory RNA of Nox4 only attenuated intracellular $O_2^{\bullet-}$ accumulation. These results suggest that Nox1 represents a major NAD(P)H oxidase isoform responsible for extracellular $O_2^{\bullet-}$ production. This rapid extracellular production of $O_2^{\bullet-}$ seems to be unique to OXO-induced M_1-receptor activation, since ANG II-induced intra- and extracellular $O_2^{\bullet-}$ increases in parallel. It is concluded that the outward production of $O_2^{\bullet-}$ via NAD(P)H oxidase in CAMs may represent an important producing pattern for its autocrine or paracrine actions.

reactive oxygen species; redox signaling; artery

SINCE THE 1970S, many studies have documented that, in the presence of an exogenous superoxide ($O_2^{\bullet-}$) donor, the action of endothelium-dependent relaxing factors could be attenuated and vasoconstriction occurred. When superoxide dismutase (SOD) was used to pretreat the arteries, this exogenous $O_2^{\bullet-}$-induced vasoconstriction or impairment of vasodilation was significantly attenuated (26, 32). In this regard, Furchgott and colleagues (22, 34) further demonstrated that addition of SOD in the bath solution of the arterial preparations to dismutate $O_2^{\bullet-}$ significantly enhanced endothelium-dependent vasodilation and increased the bioavailability of one of the endothelium-dependent relaxing factors, nitric oxide (NO). Given that SOD was added outside vascular cells in these experiments, it seems that an interaction of $O_2^{\bullet-}$ and NO would occur in the extracellular compartment or interstitial space because SOD as a protein cannot easily enter the cells. Even polyethylene glycol-SOD as used in some experiments (3, 21) may only facilitate approaches of SOD to the cell membrane in acute or short-term experimental protocols, rather than the entry of SOD into the cells. This raises several questions over the resources of $O_2^{\bullet-}$ outside vascular cells and the precise working location of extracellular $O_2^{\bullet-}$ in the vasculature. For example, where are $O_2^{\bullet-}$ anions outside vascular cells derived from? Are extracellular $O_2^{\bullet-}$ anions actively produced outward by vascular cells or passively spilled over? How could this extracellular $O_2^{\bullet-}$ production be controlled under physiological conditions? Although there are some reports indicating that vascular endothelial cells may release $O_2^{\bullet-}$ or hydrogen peroxide (H_2O_2) toward their surrounding space (16, 23), these questions are far from solved.

It has become clearer and clearer that there are several potential enzymatic sources of $O_2^{\bullet-}$ in the cardiovascular system, such as xanthine oxidase, mitochondrial respiratory chain arachidonic acid metabolizing system, uncoupled NO synthase, and NAD(P)H oxidase (43, 46). There is increasing evidence that NAD(P)H oxidase is a major source of $O_2^{\bullet-}$ in vascular cells (16, 35, 52) and that NAD(P)H oxidase-derived $O_2^{\bullet-}$ serves as an important physiological redox signaling molecule to participate in the regulation of vascular function. In vascular smooth muscle cells (VSMCs), recent studies have reported that there are membrane-bound and intracellular nonmitochondrial NAD(P)H oxidases, which are all capable of producing $O_2^{\bullet-}$ in these cells (5, 16). With various existing techniques, $O_2^{\bullet-}$ has been demonstrated to be accumulated within VSMCs when NAD(P)H oxidase is activated by different agonists such as ANG II (15). This intracellular accumulation of $O_2^{\bullet-}$ led to an assumption that a plasma membrane-bound NAD(P)H oxidase may produce and release $O_2^{\bullet-}$ into cells, which is different from the orientation of phagocyte NAD(P)H oxidases (16). However, the proposed topology of NAD(P)H oxidase subunits indicates that membrane-associated NAD(P)H oxidase should not release $O_2^{\bullet-}$ into cytosol (4,

Address for reprint requests and other correspondence: P.-L. Li, Dept. of Pharmacology and Toxicology, Medical College of Virginia, 410 North 12th St., Richmond, VA 23298 (e-mail: pli@vcu.edu).

The costs of publication of this article were defrayed in part by the payment of page charges. The article must therefore be hereby marked "*advertisement*" in accordance with 18 U.S.C. Section 1734 solely to indicate this fact.

25). Studies on subcellular localization of vascular NAD(P)H oxidase subunits also demonstrated that $O_2^{\bullet-}$ within VSMCs may not be derived from plasma membrane NAD(P)H oxidase but rather from intracellular compartmental NAD(P)H oxidase (45, 52). More recently, using patch-clamp technique, our group (30) surprisingly recorded an inward current associated with NAD(P)H oxidase in coronary arterial myocytes (CAMs) that was similar to that recorded in phagocytes, indicating that an outward electron flow and $O_2^{\bullet-}$ production occurred in these VSMCs. It seems that a membrane-bound NAD(P)H oxidase in VSMCs could generate $O_2^{\bullet-}$ toward the outside of these cells, and in this way $O_2^{\bullet-}$ may exert regulatory roles as an autocrine or paracrine.

To test this hypothesis, we first modified a high-speed wavelength-switching fluorescent microscopic imaging technique to allow a simultaneous monitoring of extracellular and intracellular $O_2^{\bullet-}$ production in single CAMs. In addition to the intracellular DNA trapping of dihydroethidium (DHE) product, a Matrigel DNA trapping around CAMs was developed to detect $O_2^{\bullet-}$-oxidized DHE signals, which represents extracellular $O_2^{\bullet-}$ levels. In addition, $O_2^{\bullet-}$-mediated precipitation from nitro blue tetrazolium (NBT) and Matrigel-trapped OxyBURST H_2HFF Green BSA staining around CAMs were also determined by light or confocal fluorescent microscopy, respectively. Using electron spin resonance (ESR) spectrometric measurement, we examined whether SOD-sensitive extracellular $O_2^{\bullet-}$ changes could be detected. After we confirmed the extracellular production of $O_2^{\bullet-}$ in response to activation of M_1-muscarinic receptor, we observed the effects of $O_2^{\bullet-}$ scavengers or specific NAD(P)H oxidase inhibitors on intracellular and extracellular $O_2^{\bullet-}$ production and also dissected the contribution of different NAD(P)H oxidase isoforms to this agonist-induced redox response by RNA interference with specific, small inhibitory RNAs (siRNAs). We then went on to examine whether $O_2^{\bullet-}$ outward production in response to M_1-muscarinic activation occurs when CAMs were stimulated by other agonists, in particular ANG II. Our results suggest that activation of NAD(P)H oxidase gives rise to a different spatiotemporal pattern of $O_2^{\bullet-}$ production when these cells are exposed to different stimuli. Most importantly, our experiments provide direct evidence at the single cell level that the outward production of $O_2^{\bullet-}$ associated with NAD(P)H oxidase occurs in CAMs, which may exert autocrine or paracrine actions in the redox regulation of vascular function.

MATERIALS AND METHODS

Isolation and culture of CAMs. As our group described previously (41), fresh bovine hearts were obtained from a local abattoir, and intramyocardial coronary arteries from the branches of left anterior descending artery were rapidly dissected. Endothelium-denuded coronary arteries were rinsed with medium 199 containing 5% FBS, a 2% solution of antibiotics (penicillin-streptomycin), 0.3% gentamicin, and 0.3% nystatin and cleaned of connective tissues. After they were cut into small pieces, the arteries were placed into dishes with the lumen side down and incubated in medium 199 containing 10% FBS, 1% glutamine, 1% antibiotic solution, 0.3% gentamicin, 0.3% nystatin, and 0.1% tylosin for 3–5 days until vascular myocytes migrated to the dishes. Once CAM growth had been established, the vessels were removed, and the cells were grown in medium 199 containing 20% FBS. All cells were maintained in an incubator with 5% CO_2 in air at 37°C. The CAMs were identified by positive staining with an anti-α-actin antibody. All studies were performed with cells of *passages 2–4*.

Simultaneously monitoring $O_2^{\bullet-}$ production inside and outside CAMs. This method is based on the DNA binding characteristic of oxidized DHE product ethidium in intracellular DNA and Matrigel-trapped extracellular DNA when CAMs were stimulated by different agonists. This DNA binding assay of $O_2^{\bullet-}$, which oxidizes DHE to produce a strong red fluorescence, is widely used for intracellular $O_2^{\bullet-}$ production in the vessel wall and in isolated vascular endothelial and VSMCs (6, 40). However, this DNA-ethidium binding assay has not yet been used to detect extracellular $O_2^{\bullet-}$ at the single cell level. The major challenge is how to trap DNA outside the cells. To solve this problem, we have used Matrigel (BD Biosciences) as a supportive matrix to trap DNA that is capable of binding to the ethidium from oxidation of DHE in solution. In these experiments, isolated CAMs (10^2 cells/well) were seeded into a 16-well chamber slide with a transparent glass bottom (LAB-TEK) and incubated overnight to attach the bottom of the wells. On the day of experiments, the culture medium was first discarded, CAMs were washed twice with Hanks' buffer, and 40 μl of salmon testes DNA solution (7.5 mg/ml; Sigma) were mixed with 40 μl of Matrigel solution (at 4°C) and then were carefully loaded onto the top of CAMs. After 5 min at room temperature, the gel was polymerized and exogenous DNA was immobilized around these cells. The CAMs with Matrigel were then filled with Hanks' buffer containing 250 μM DHE. After a 60-min loading of DHE into the CAMs, the chamber slide was mounted on the stage of a fluorescent microscope that we routinely used for high-speed wavelength-switching imaging acquisition and recording. For both intracellular and extracellular DHE oxidizing signals, a ratio of ethidium-DNA to DHE signals was recorded (ethidium-DNA fluorescence signal was detected at an excitation of 480 nm and an emission of 610 nm, and DHE fluorescence signal was detected at an excitation of 380 nm and an emission of 445 nm). For each experiment, 8–10 CAMs were monitored simultaneously and an average value was used for statistical analysis.

The M_1-receptor agonist oxotremorine (OXO; 80 μM) was added to activate its receptor and consequently stimulate $O_2^{\bullet-}$ production. In the groups of CAMs receiving $O_2^{\bullet-}$ scavengers or NAD(P)H oxidase inhibitors, SOD (500 U/ml) plus catalase (400 U/ml), diphenylene iodonium (DPI; 50 μM), or apocynin (100 μM) was preincubated with the cells for 15 min, and then the $O_2^{\bullet-}$-producing response to OXO was determined. In addition, a time course of NAD(P)H oxidase activation and intracellular and extracellular $O_2^{\bullet-}$ production in response to ANG II was monitored, when this peptide was added into the well containing Matrigel and cells at a concentration of 100 nM. All doses of these agonists or inhibitors used in the present experiments were based on previous studies reported by our laboratory and other laboratories.

NBT precipitation detection of extracellular $O_2^{\bullet-}$. As described in previous studies (13), $O_2^{\bullet-}$ accumulation outside CAMs was also determined with NBT, which reacts with $O_2^{\bullet-}$ and produces a blue formazin precipitate. NBT (0.1%) was prepared in PBS by adding 10 mg of NBT powder (Sigma) to 100 ml of PBS (pH 7.2) and stirred at room temperature for 1 h. NBT staining was then performed by adding 0.1% of NBT solution into a well seeded with CAMs and incubated for 30 min at 37°C before and after addition of OXO (80 μM). Under ×100 magnification microscopy (Nikon), two-dimensional optical images were acquired with a digital camera (Spot).

Confocal microscopic detection of extracellular $O_2^{\bullet-}$. To further determine extracellular $O_2^{\bullet-}$, CAMs were prepared as described above for ethidium-DNA trapping imaging. In brief, 0.5 ml of Matrigel was mixed with 25 μl of OxyBURST H_2HFF Green BSA (10 μg/ml; Molecular Probes) and then used to evenly coat the 35 mm × 10-mm cell culture dish. Freshly isolated CAM suspension (60 μl) was loaded on the top of the ice-cold Matrigel matrix, and then the culture dish was gently tapped three or four times to sit cells on the surface of the gel. At room temperature, the gel was polymerized in ~5 min. Then, 2 ml of Krebs-Ringer phosphate buffer, which contains PBS, pH 7.4, with 1.0 mM Ca^{2+}, 1.5 mM Mg^{2+}, and 5.5 mM glucose,

were added. Confocal fluorescent microscopic images were acquired by an Olympus Fluoview system (version 4.2, FV300), consisting of an Olympus BX61WI inverted microscope with an Olympus Lumplan F1 ×60, 0.9 numerical aperture, water-immersion objective. A single *z*-section was taken, or 0.1-μm sections were obtained through the cell with excitation and emission wavelengths of 488 and 530 nm, respectively, for OxyBURST. Real-time microscopic fluorescence images were acquired every 1 or 2 min under control conditions and after different treatments. This OxyBURST H_2HFF Green BSA detects H_2O_2, which mirrors $O_2^{\bullet-}$ production outside the cells because BSA cannot enter the cells (8).

ESR detection of extracellular $O_2^{\bullet-}$. For extracellular $O_2^{\bullet-}$ assay, gently collected CAMs were suspended in modified Krebs-HEPES buffer containing deferoxamine (100 μM; metal chelator). Approximately 1×10^6 cells were then incubated with OXO (80 μM) or ANG II (100 nM) for 30 min; these were subsequently mixed with 1 mM of the $O_2^{\bullet-}$-specific spin trap 1-hydroxy-3-methoxycarbonyl-2,2,5,5-tetramethylpyrrolidine (CMH) in the presence or absence of manganese-dependent SOD (500 U/ml). The cell mixture was then loaded in glass capillaries and immediately kinetically analyzed for $O_2^{\bullet-}$ production for 10 min. The SOD-inhibitable fraction of the signal was compared. The ESR settings were as follows: biofield, 3,350; field sweep, 60 G; microwave frequency, 9.78 GHz; microwave power, 20 mW; modulation amplitude, 3 G; 4,096 points of resolution; receiver gain, 100; and kinetic time, 10 min (7).

RNA interference and Nox1, Nox4, and p47^{phox} gene in CAMs. To dissect the role of different NAD(P)H oxidase subunits in OXO-induced or ANG II-induced $O_2^{\bullet-}$ production outside or inside CAMs, RNA interference was performed to silence the gene coding these subunits. Three pairs of siRNAs were designed and targeted, including p47 (AAAGGGCTCGAGTTCCCAAAT), Nox1 (AAGGGCTTTCGAACAACAATA), Nox4 (AAGACCTGGCCAGTATATTAT), and Nox2 (AAGTCGGTCTGGTACAAATAT). Selection of these NAD(P)H oxidase subunits was based on previous studies that indicated that these may contribute to the activity of membrane-bound and cytosolic compartmental components of NAD(P)H oxidases (20, 45). In these experiments, siRNA transfection was performed according to the manufacturer's instruction in Qiagen TransMessenger kit. All siRNAs were chosen with a Qiagen siRNA design program and synthesized and double-stranded by Xeragon. A scrambled, small RNA was synthesized for a negative control.

Statistics. Data are expressed as means ± SE. The significance of the differences in mean values between and within multiple groups such as multiple time points was examined by ANOVA for repeated measures followed by Duncan's multiple range test. Student's *t*-test was used to evaluate the statistical significance of differences between two paired observations. $P < 0.05$ was considered statistically significant.

RESULTS

Spatiotemporal pattern of $O_2^{\bullet-}$ production by CAMs in response to OXO. Using the high-speed wavelength-switching technique, we simultaneously monitored the fluorescence intensity of ethidium-DNA complex within primary cultures of CAMs and in Matrigel around these cells. Figure 1*A* shows typical fluorescent images acquired during 30 min when a CAM received OXO at a concentration of 80 μM. It was found that, at the first 10 min of incubation with OXO, $O_2^{\bullet-}$ levels increased with a predominate response outside cells (becoming red). Starting at 15 min of OXO incubation, intracellular fluorescence intensity increased when the outside signal became much stronger. At ~30 min of OXO incubation, intracellular fluorescence became as intense as those observed outside cells. This dynamic change in intracellular and extracellular ethidium-DNA fluorescence was digitized and acquired by using a MetaFluor program (version 6.2). Summarized results are presented in Fig. 1*B*. It was clear that OXO produced a more rapid increase in ethidium-DNA fluorescence outside CAMs than inside these cells. At 30 min of OXO incubation, the intracellular signal reached a level similar to that observed outside CAMs. In addition, we also monitored similar changes in dynamic responses of intracellular and extracellular ethidium-DNA fluorescence in freshly isolated CAMs in response to OXO (data not shown).

In the presence of SOD (500 U/ml) in the chamber solution, OXO-induced increases in $O_2^{\bullet-}$ levels both inside and outside CAMs were completely blocked (remained blue, as shown in Fig. 1*A*). As summarized in Fig. 1*C*, $O_2^{\bullet-}$ increases induced by OXO both outside and inside CAMs were blocked by extracellular SOD + CAT (400 U/ml), but not by CAT alone, suggesting that these signals are specific to $O_2^{\bullet-}$ production. It should be noted that the blockade of intracellular $O_2^{\bullet-}$ production by extracellular SOD in this preparation may be associated with a triggering or activating action of $O_2^{\bullet-}$ on intracellular NAD(P)H oxidase through different pathways such as PKC and ion channels (19, 42). Therefore, when SOD dismutates $O_2^{\bullet-}$ outside CAMs, this activation of intracellular NAD(P)H oxidase was simultaneously blocked.

To address a concern regarding whether a rapid increase in extracellular fluorescent signal in response to OXO stimulation may be due to the different speeds of ethidium binding to intracellular DNA or extracellular DNA in Matrigel, we performed a similar recording with substitution of intracellular 2′,7′-dichlorofluorescin diacetate (H_2DCFDA, a cell-permeant indicator for reactive oxygen species) for DHE, where H_2DCFDA in cytosol directly reacts with H_2O_2. The results showed a similar pattern of intracellular and extracellular changes in $O_2^{\bullet-}$ production in response to OXO (data not shown), where the extracellular increase in fluorescent signal was more rapid than the intracellular increase.

NBT precipitation. As shown in Fig. 2*A*, using NBT staining, we found that dark blue precipitations were significantly increased when CAMs were incubated with OXO. These experiments were performed to further confirm an extracellular production of $O_2^{\bullet-}$. As mentioned above, NBT in the bath solution could be reduced by reactive oxygen species (ROS) to dark blue, insoluble formazin-NBT, producing dark blue particles outside the cells. This dye is widely used to detect activation of NAD(P)H oxidase in different cells (12, 18). Although NBT may not be used to specifically dissect which ROS molecules are produced outside CAMs, when it was reduced and precipitated in these experiments, it is indicative for $O_2^{\bullet-}$ production under these conditions.

Confocal microscopic detection of extracellular OxyBURST Green H_2HFF BSA. Another approach that we used to further detect extracellular $O_2^{\bullet-}$ levels is confocal microscopic analysis of OxyBURST Green H_2HFF BSA. This BSA-conjugated fluorescent dye is primarily used to detect extracellular ROS by illustrating H_2O_2. Because BSA cannot enter cells, the detected green fluorescence in Matrigel around CAMs represents extracellular ROS. Although it might not detect $O_2^{\bullet-}$, this fluorescence intensity reflects $O_2^{\bullet-}$-derived ROS levels. As shown in Fig. 2*B*, OXO markedly increased green fluorescence in Matrigel containing OxyBURST Green H_2HFF BSA, which was blocked completely by SOD and catalase.

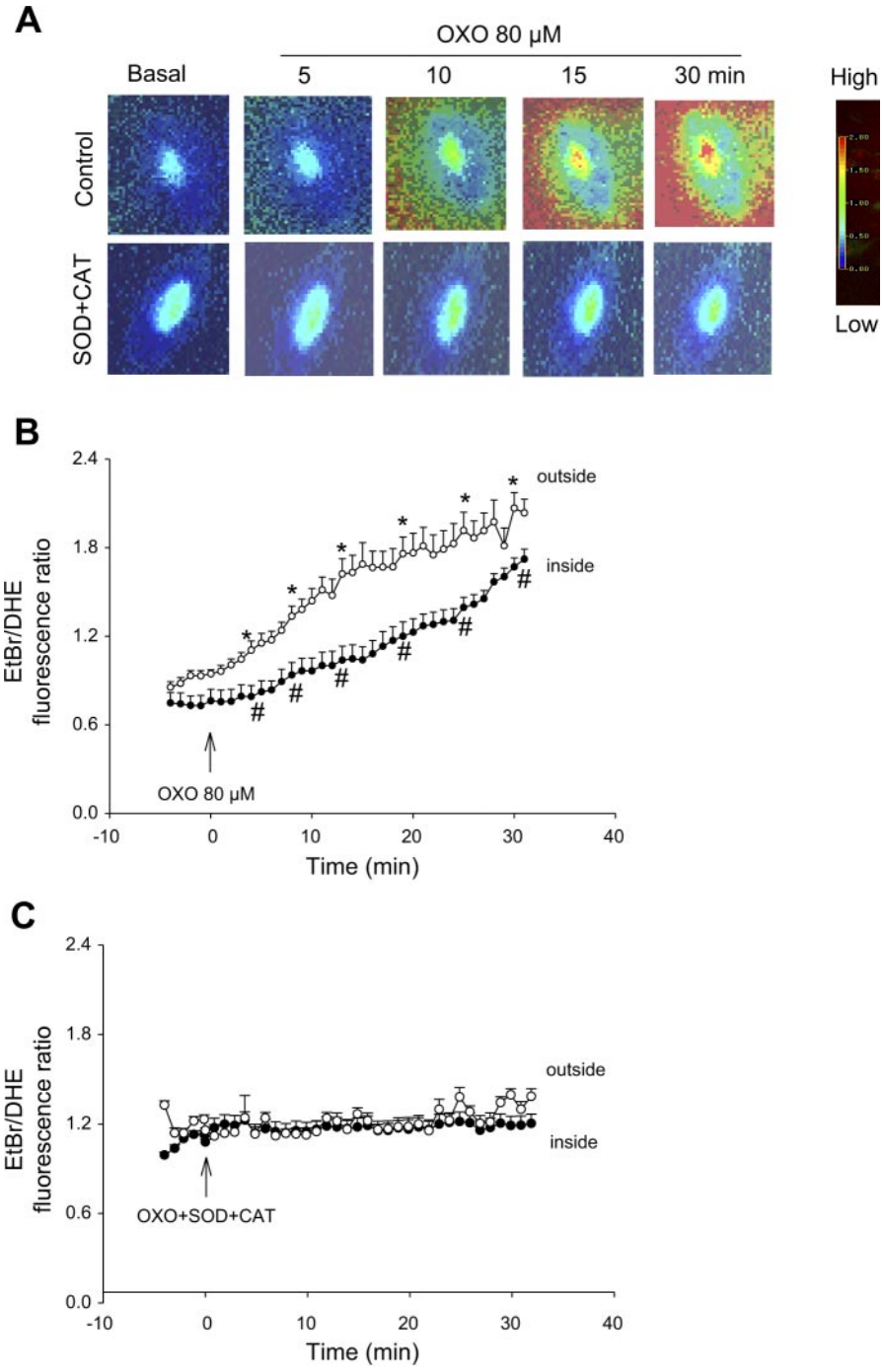

Fig. 1. Fluorescent microscopic imaging analysis to simultaneously monitor oxotremorine (OXO)-induced superoxide ($O_2^{\bullet-}$) production inside and outside single coronary arterial myocytes (CAMs). *A*: typical time-dependent increase in oxidized dihydroethidium (DHE) fluorescence ratio [ethidium bromide (EtBr)/DHE] image inside and outside a CAM in the presence or absence of superoxide dismutase (SOD; 500 U/ml). Red fluorescence image indicates $O_2^{\bullet-}$ level higher than blue background. *B*: summarized digitized data showing the spatiotemporal pattern of $O_2^{\bullet-}$ increase outside and inside CAMs during OXO (80 μM) stimulation. *C*: spatiotemporal pattern of $O_2^{\bullet-}$ increase outside and inside CAMs during OXO stimulation after treatment with SOD (500 U/ml) in combination with catalase (CAT; 400 U/ml) ($n = 6$ cases). *$P < 0.05$ compared with control (at 0 min); #$P < 0.05$ compared with values obtained outside CAMs.

ESR measurements of extracellular $O_2^{\bullet-}$ levels. Using ESR spectrometric assay, we demonstrated the $O_2^{\bullet-}$ production and release from CAMs in response to OXO. In these experiments, a 30-min incubation of OXO with CAMs elicited a typical ESR signal resulting from the CMH trapping, which was measured from cultured CAMs rapidly collected after exposure to OXO. The SOD-inhibitable fraction of the signal, specifically reflecting extracellular $O_2^{\bullet-}$ production, was compared. Figure 3*A* depicts representative changes in SOD-inhibitable ESR spectrometric curve recorded under control conditions and after treatment of cells with OXO (80 μM) or ANG II (100 nM). Summarized data from these experiments showed that both OXO and ANG II significantly increased production of $O_2^{\bullet-}$ outside CAMs (Fig. 3*B*). At 10 min, a more than threefold increase in extracellular $O_2^{\bullet-}$ production was observed in these ANG II- or OXO-treated CAMs.

Effects of NAD(P)H oxidase inhibitors on OXO-induced $O_2^{\bullet-}$ production. To determine whether the $O_2^{\bullet-}$ production increase was derived from NAD(P)H oxidase, we examined the effects of two general NAD(P)H oxidase inhibitors, DPI or apocynin, on $O_2^{\bullet-}$ levels inside and outside CAMs during OXO stimulation using fluorescent microscopic imaging technique. It was found that incubation of CAMs with DPI (50 μM) significantly blocked the maximal increase in intracellular

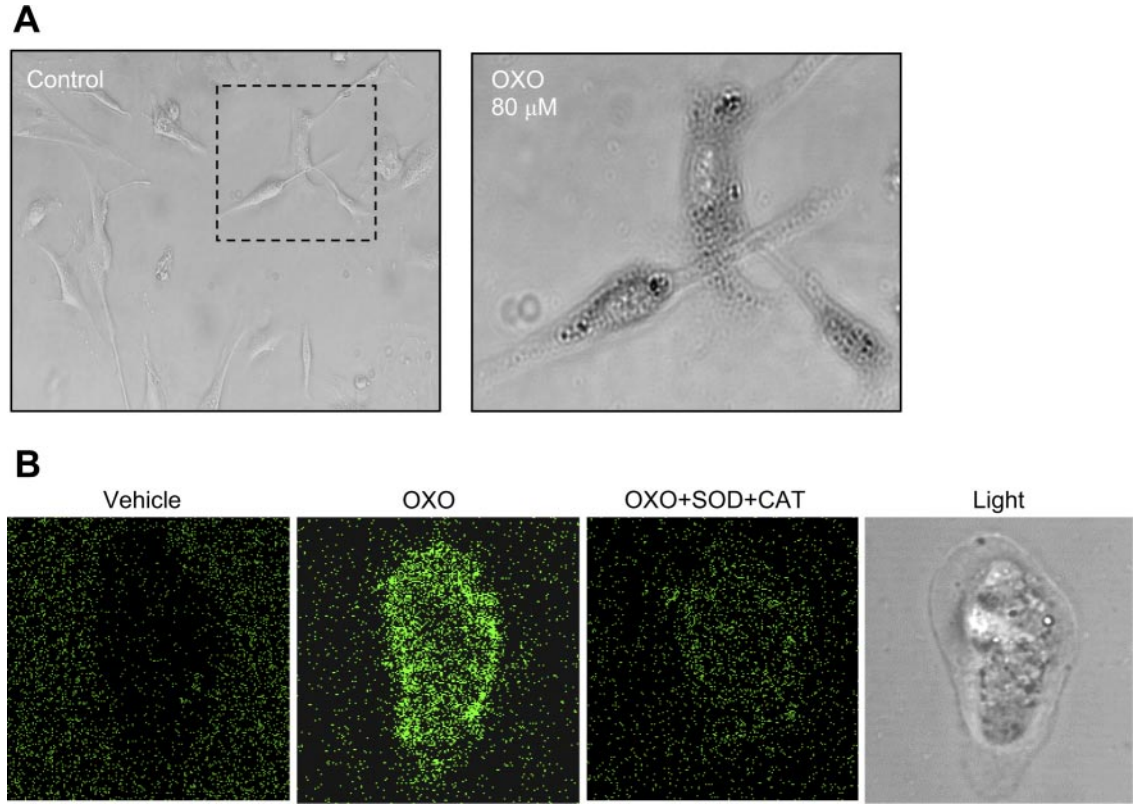

Fig. 2. Microscopic confirmation of extracellular $O_2^{\bullet-}$ production in CAMs. *A*: nitro blue tetrazolium staining, where dark blue precipitations were found outside CAMs when they were stimulated by OXO (80 μM). *B*: confocal fluorescent images showing extracellular $O_2^{\bullet-}$ production as measured by OxyBURST Green H_2HFF BSA trapped H_2O_2 outside a CAM exposed to OXO (80 μM) in the absence or presence of SOD (500 U/ml) plus CAT (400 U/ml) (n = 5 cases).

and extracellular $O_2^{\bullet-}$ levels induced by OXO by 76% and 37%, respectively. It should be noted that the early response of $O_2^{\bullet-}$ production to OXO was almost blocked by DPI (Fig. 4*A*). A similar inhibitory effect of apocynin (100 μM) on OXO-induced $O_2^{\bullet-}$ production was also observed (Fig. 4*B*).

Effects of gene silencing of NAD(P)H oxidase subunits on OXO-induced $O_2^{\bullet-}$ production. RNA interference experiments were performed as described in our previous studies for antisense oligodeoxynucleotides or decoy of transcription factors in different cells (48, 49). The transfection rate of siRNA with liposomes was ~70% CAMs as detected by fluorescent microscopy of fluorescein-labeled scrambled, small RNA. In CAMs with Nox1 siRNA transfection, both intracellular and extracellular $O_2^{\bullet-}$ production as measured by ethidium-DNA fluorescence was significantly less than in CAMs with scrambled, small RNAs (Fig. 5*A*). However, silencing Nox4 in CAMs only significantly reduced intracellular $O_2^{\bullet-}$ production, but it had no effect on $O_2^{\bullet-}$ levels detected outside these Nox4-silenced CAMs (Fig. 5*B*). When the gene of $p47^{phox}$ subunit was silenced, both intra- and extracellular $O_2^{\bullet-}$ productions were markedly attenuated (Fig. 5*C*). However, Nox2 siRNA had no significant effect on intra- or extracellular $O_2^{\bullet-}$ production induced by OXO (data not shown).

Effects of exogenous $O_2^{\bullet-}$ on intracellular NAD(P)H oxidase activity. In these experiments, X (100 μM)/XO (0.1 mU/ml) was added into the bath solution in the preparation used for extracellular and intracellular $O_2^{\bullet-}$ assay as shown in Fig. 1 to determine whether exogenous $O_2^{\bullet-}$ stimulates an activation of intracellular NAD(P)H oxidase. As shown in Fig. 6, X/XO significantly induced $O_2^{\bullet-}$ production with a pattern similar to that of OXO, namely, rapid increase in extracellular $O_2^{\bullet-}$ followed by a sustained increase in intracellular $O_2^{\bullet-}$ (Fig. 6*A*). This intracellular increase in $O_2^{\bullet-}$ levels induced by X/XO was significantly attenuated by NAD(P)H oxidase inhibitor DPI (Fig. 6*B*) or apocynin (Fig. 6*C*). However, increases in extracellular $O_2^{\bullet-}$ produced by X/XO were not altered by either DPI or apocynin.

Spatiotemporal pattern of ANG II-induced $O_2^{\bullet-}$ production in CAMs. These experiments were done to determine whether a more rapid $O_2^{\bullet-}$ production outside than inside cells also occurs in response to other agonists such as ANG II. As conducted in OXO experiments using the high-speed wavelength-switching technique of fluorescent microscopic imaging, both intracellular and extracellular $O_2^{\bullet-}$ production were simultaneously monitored. Figure 7*A* presents a typical 30-min dynamic change in fluorescent images indicating $O_2^{\bullet-}$ production inside and outside CAMs in response to ANG II. In contrast to the findings that OXO induced an increase in $O_2^{\bullet-}$ signals outside CAMs more rapidly than inside these cells, ANG II produced a parallel increase in fluorescence intensity both outside and inside the cells. The results are summarized in Fig. 7*B*, showing that intracellular and extracellular $O_2^{\bullet-}$ production in response to ANG II was similar in magnitude to that induced by OXO. In the presence of SOD (500 U/ml) and catalase (400 U/ml) outside these cells, ANG II-induced increases in $O_2^{\bullet-}$ levels both inside and outside cells were completely blocked (Fig. 7*C*). However, CAT alone had no

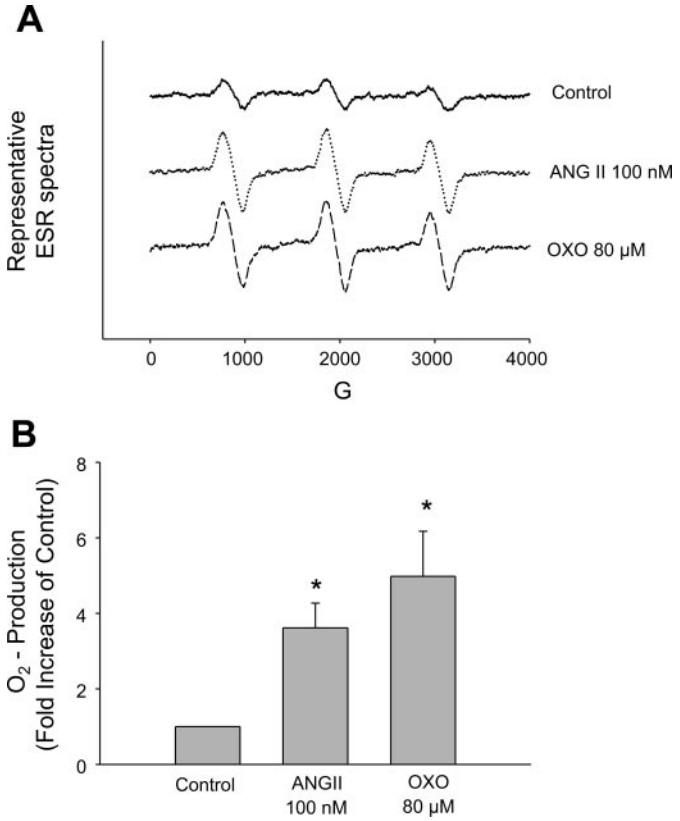

Fig. 3. Electron spin resonance (ESR) spectrometric assay of extracellular $O_2^{\bullet-}$ levels produced by CAMs. *A*: representative ESR spectrograph of $O_2^{\bullet-}$ trapped by 1-hydroxy-3-methoxycarbonyl-2,2,5,5-tetramethylpyrrolidine (CMH) showing SOD-sensitive component of signals recorded under control conditions and after treatment of cells with OXO (80 μM) or ANG II (100 nM). *B*: summarized data showing ANG II or OXO-induced $O_2^{\bullet-}$ production ($n = 6$ cases). $^*P < 0.05$ compared with control.

effect on ANG II-induced increases in $O_2^{\bullet-}$ levels either inside or outside these cells.

Effects of NAD(P)H oxidase inhibitors on ANG II-induced $O_2^{\bullet-}$ production. Similar to the results observed in experiments that used OXO as stimuli, the NAD(P)H oxidase inhibitors DPI (50 μM) and apocynin (100 μM) substantially blocked ANG II (100 nM)-induced increases in intracellular and extracellular $O_2^{\bullet-}$ levels (Fig. 8). The early-stage increases in $O_2^{\bullet-}$ production both outside and inside CAMs in response to ANG II were also almost completely abolished.

Effects of gene silencing of NAD(P)H oxidase subunits on ANG II-induced $O_2^{\bullet-}$ production. Similar to the results obtained in experiments that used OXO as stimuli, Nox1 siRNA attenuated ANG II-induced increase in extracellular $O_2^{\bullet-}$ levels in CAMs by 46%, whereas Nox4 siRNA substantially decreased intracellular $O_2^{\bullet-}$. Moreover, in the presence of $p47^{phox}$ siRNA, both intra- and extracellular $O_2^{\bullet-}$ production in these cells in response to ANG II markedly decreased (Fig. 9). These data suggest that siRNAs of different subunits or isoforms of NAD(P)H oxidase have similar blocking action on agonist responses no matter whether OXO or ANG II was used. However, Nox1 and Nox4 seem to have different contributions to extracellular or intracellular $O_2^{\bullet-}$ production. In additional experiments, Nox2 siRNA was not found to have any significant action on extracellular and intracellular $O_2^{\bullet-}$ production in response to ANG II (data not shown).

DISCUSSION

Despite overwhelming evidence that NAD(P)H oxidase-derived $O_2^{\bullet-}$ importantly participates in the regulation of vascular function under physiological conditions and that this enzymatic $O_2^{\bullet-}$ production from vascular cells is involved in the development of various vascular diseases such as atherosclerosis (53), hypertension, and diabetic vasculopathy (10, 54), the mechanisms activating and regulating the activity of this enzyme are still poorly understood. With a highly sensitive fluorescent imaging technique, the present study analyzed a spatiotemporal pattern of $O_2^{\bullet-}$ production at the single cell level and demonstrated the NAD(P)H oxidase-associated outward production of $O_2^{\bullet-}$ in CAMs when these cells were stimulated under a relatively physiological condition by M_1 agonist OXO and ANG II. This outward production of $O_2^{\bullet-}$ was confirmed with a variety of ROS detection methods. It was also found that the spatiotemporal pattern of $O_2^{\bullet-}$ of CAMs in response to OXO or ANG II was different, in which OXO produced a more rapid increase in $O_2^{\bullet-}$ levels outside than inside CAMs, whereas ANG II induced a parallel increase in $O_2^{\bullet-}$ levels both outside and inside these cells. In addition, the

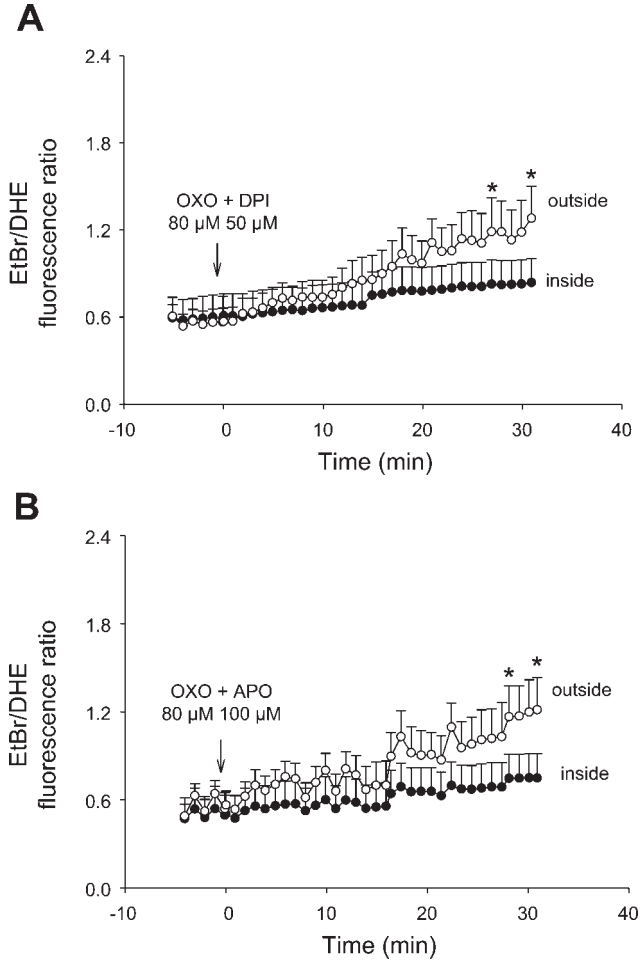

Fig. 4. Effects of NAD(P)H oxidase inhibitor on OXO-induced $O_2^{\bullet-}$ production inside and outside CAMs as measured by fluorescent microscopic imaging analysis. *A*: inhibition of OXO (80 μM)-induced $O_2^{\bullet-}$ production by diphenylene iodonium (DPI; 50 μM) ($n = 6$ cases). *B*: inhibition of OXO-induced $O_2^{\bullet-}$ production by apocynin (APO; 100 μM) ($n = 6$ cases). $^*P < 0.05$ compared with control (at 0 min).

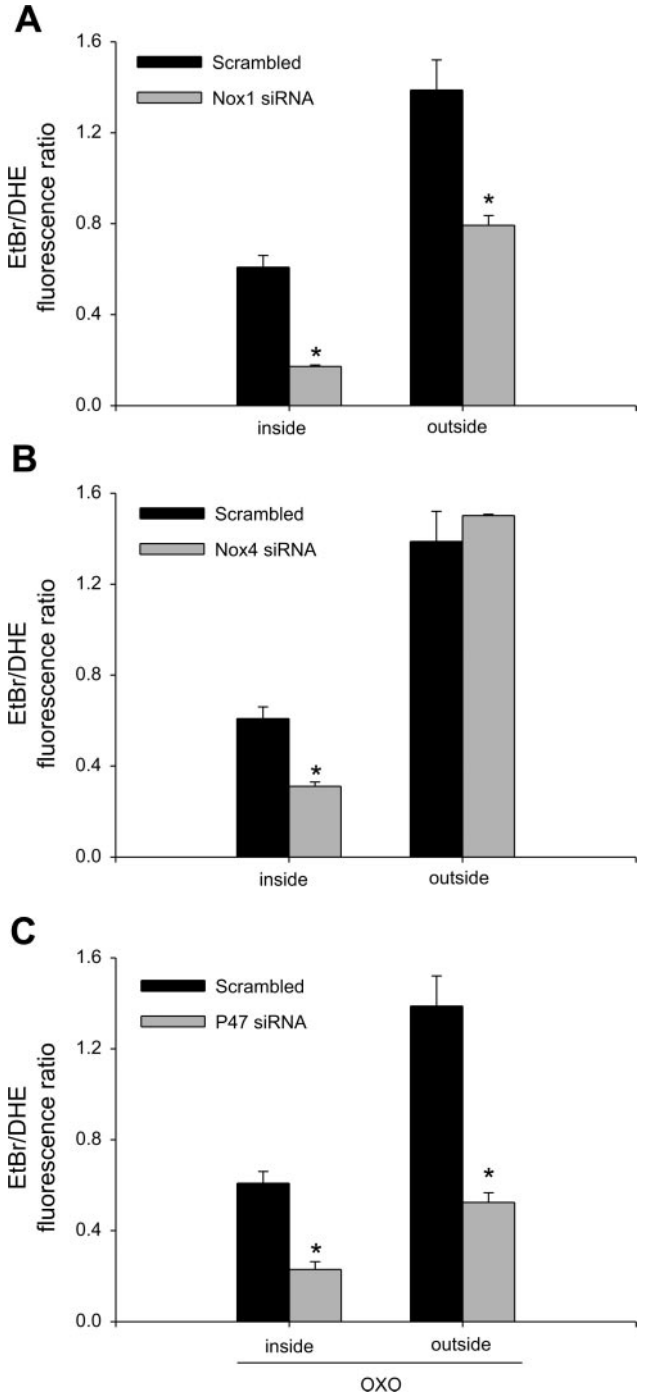

Fig. 5. Effects of RNA interference on OXO (80 μM)-induced $O_2^{\bullet-}$ production inside and outside CAMs as measured by fluorescent microscopic imaging analysis. *A*: effect of Nox1 small inhibitory RNA (siRNA) or scrambled, small RNA ($n = 6$ cases). *B*: effect of Nox4 siRNA or scrambled, small RNA ($n = 6$ cases). *C*: effect of $p47^{phox}$ siRNA or scrambled, small RNA ($n = 6$ cases). $^*P < 0.05$ compared with values obtained from CAMs treated with scrambled, small RNA.

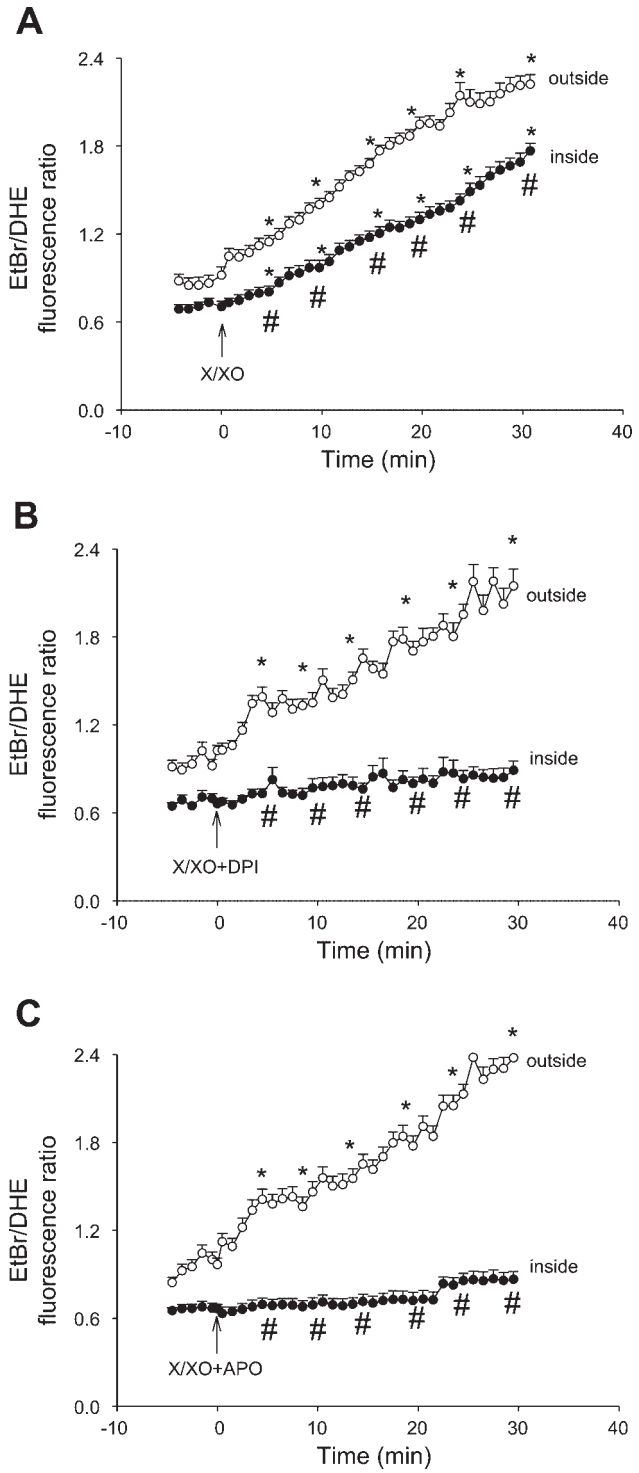

Fig. 6. Fluorescent microscopic imaging analysis to simultaneously monitor X/XO-induced $O_2^{\bullet-}$ production inside and outside single CAMs. *A*: time-dependent increase in oxidized DHE fluorescence ratio (EtBr/DHE) inside and outside CAMs before and after treatment with X (100 μM)/XO (0.1 mU/ml). *B*: in the presence of DPI (50 μM), X/XO induced EtBr/DHE signal inside and outside CAMs. *C*: in the presence of APO (100 μM), X/XO induced EtBr/DHE signal inside and outside CAMs. In *A–C*, $n = 6$ cases. $^*P < 0.05$ compared with control (at 0 min); $\#P < 0.05$ compared with values obtained outside CAMs.

present study demonstrated that Nox1 may be the major isoform responsible for the increase in the extracellular $O_2^{\bullet-}$ level, whereas Nox4 primarily contributes to the increased intracellular $O_2^{\bullet-}$ level.

It should be noted that the major goal of our study is to determine the role of $O_2^{\bullet-}$ in the rapid and early vasomotor

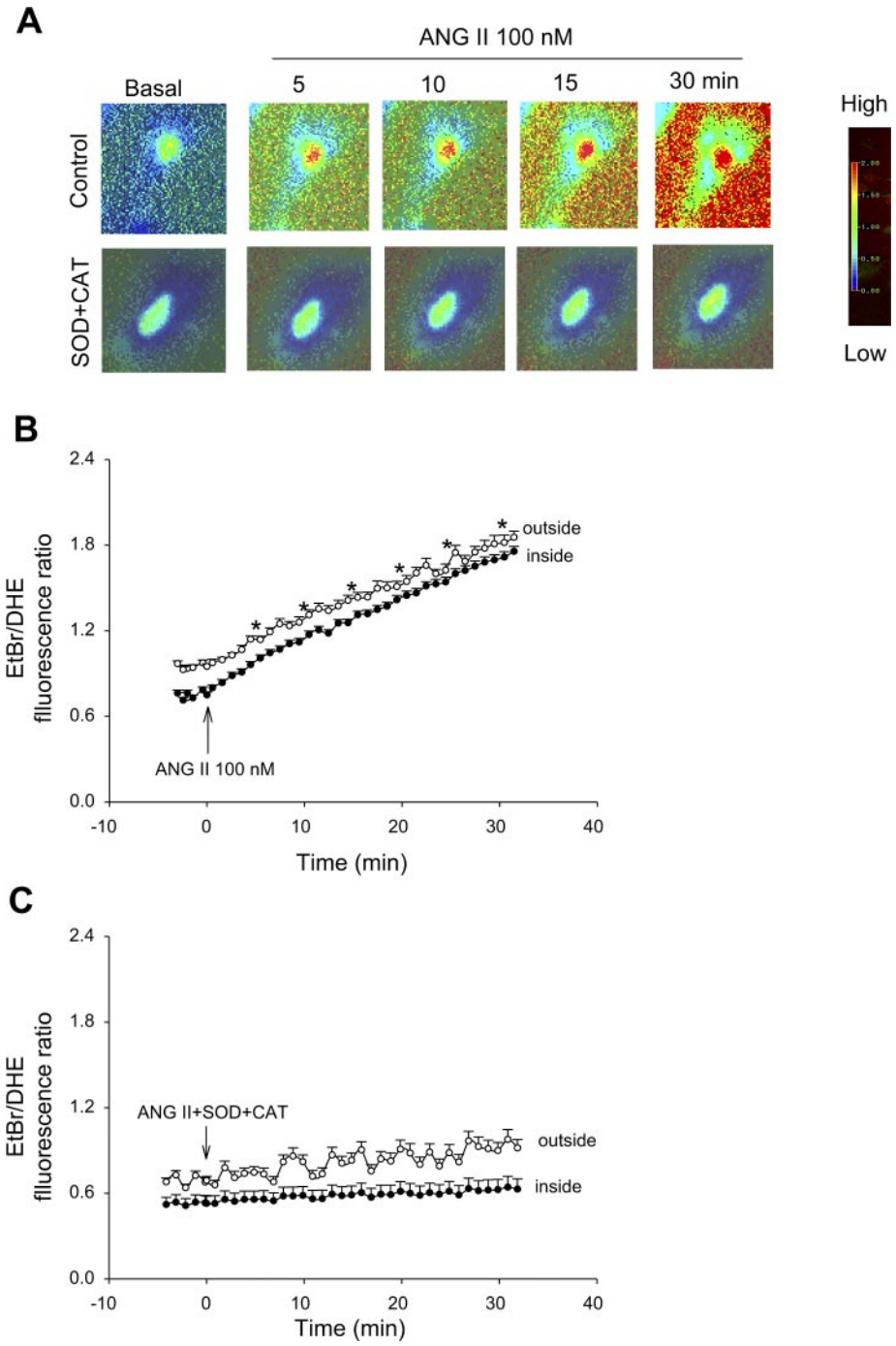

Fig. 7. Fluorescent microscopic imaging analysis to simultaneously monitor ANG II (100 nM)-induced $O_2^{\bullet-}$ production inside and outside CAMs. *A*: typical time-dependent increase in oxidized DHE fluorescence ratio (EtBr/DHE) image inside and outside CAM in the presence or absence of SOD (500 U/ml). Red fluorescence image indicates $O_2^{\bullet-}$ level higher than blue background. *B*: summarized digitized data showing the spatiotemporal pattern of $O_2^{\bullet-}$ increase outside and inside CAMs during ANG II stimulation. *C*: spatiotemporal pattern of $O_2^{\bullet-}$ increase outside and inside CAMs during ANG II stimulation after treatment with SOD (500 U/ml) in combination with CAT (400 U/ml) ($n = 6$ cases). *$P < 0.05$ compared with control (at 0 min).

responses to different agonists. Although many activators can stimulate $O_2^{\bullet-}$ production, they are usually used to stimulate vascular $O_2^{\bullet-}$ generation or accumulation for a relatively longer time. On the basis of our previous studies, bovine coronary arteries did not produce vasoconstrictor responses to many agonists such as ANG II, norepinephrine, TNF-α, Fas ligand, and other inflammatory cytokines (56, 57). In preliminary experiments, we tried several vasoconstrictors of bovine coronary arteries, including OXO, U-46619, KCl, and $CaCl_2$, which all caused $O_2^{\bullet-}$ production. Therefore, OXO was chosen as a prototype agonist of bovine coronary vasoconstrictors, which has been often used in previous studies (14, 27, 47). Although ANG II does not strongly constrict bovine coronary arteries, it was used for comparison with OXO in the present study because it has been extensively used as an NAD(P)H oxidase stimulator.

To study the spatiotemporal pattern of $O_2^{\bullet-}$ production associated with NAD(P)H oxidase activity, a sensitive and dynamic measurement of $O_2^{\bullet-}$ both inside and outside cells is needed. By modification of a high-speed wavelength-switching fluorescent microscopic imaging system that we used for simultaneous monitoring of Ca^{2+} and NO in vascular cells (51) and with the help of Matrigel to trap DNA around CAMs, we

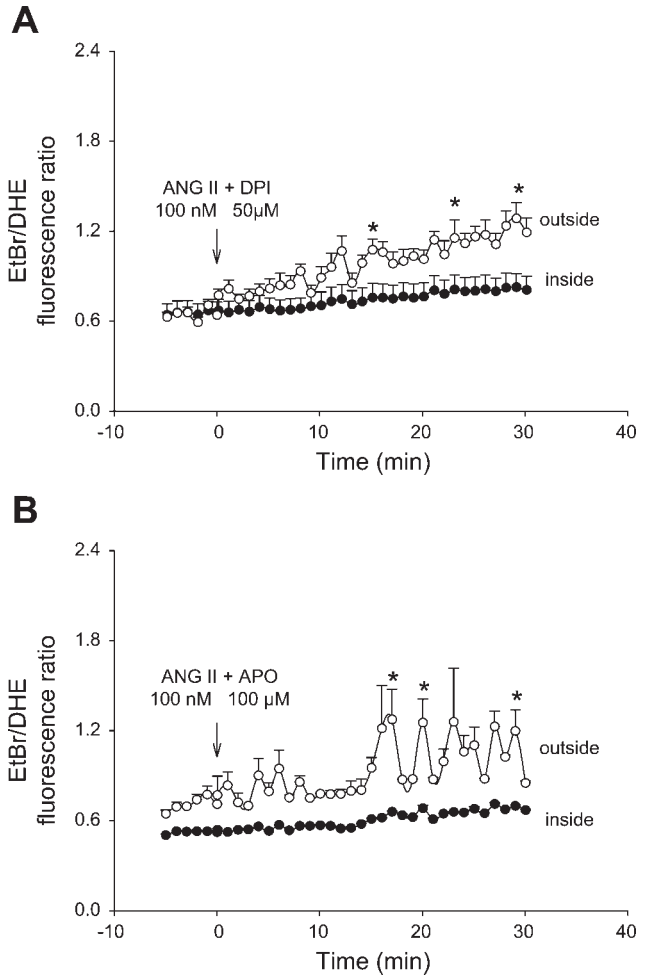

Fig. 8. Effects of NAD(P)H oxidase inhibitor on ANG II (100 nM)-induced $O_2^{\bullet-}$ production inside and outside CAMs as measured by fluorescent microscopic imaging analysis. *A*: inhibition of ANG II-induced $O_2^{\bullet-}$ production by DPI (50 μM) ($n = 6$ cases). *B*: inhibition of ANG II-induced $O_2^{\bullet-}$ production by APO (100 μM) ($n = 6$ cases). *$P < 0.05$ compared with control (at 0 min).

developed a highly sensitive imaging method to simultaneously monitor extracellular and intracellular DHE-oxidizing signals, which represent $O_2^{\bullet-}$ levels. In these experiments, Matrigel as a supportive matrix trapped DNA that is capable of binding to ethidium from oxidation of DHE in solution, and a ratio of ethidium-DNA to DHE fluorescent signals was recorded to represent $O_2^{\bullet-}$. This ratiometric assay of $O_2^{\bullet-}$ levels using DHE was used in our previous study and by others (36, 55); this method increases the sensitivity for $O_2^{\bullet-}$ detection and avoids an artifact in assays from cell volume changes or contractions during agonist stimulation. By high-speed wavelength switching, extracellular and intracellular signals can be simultaneously recorded. Using this record system, we first found that, in response to M_1-receptor activation, extracellular and intracellular $O_2^{\bullet-}$ signals could be resolved in a time-dependent manner, which was blocked by the presence of SOD and CAT, suggesting that this assay can be used for dynamic analyses of $O_2^{\bullet-}$ production. In particular, it seems that the system is sensitive for detecting $O_2^{\bullet-}$ production of a single cell at an early stage of stimulation by M_1 agonist. In previous studies, although DHE-based assay was used for a variety of samples or preparations for detection of intracellular $O_2^{\bullet-}$, a dynamic observation of $O_2^{\bullet-}$ production within a short time period of 10 or 30 min could not be resolved (2). More importantly, simultaneously monitoring of $O_2^{\bullet-}$ increases inside and outside CAMs in response to M_1 agonist provides an important tool to study the orientation of $O_2^{\bullet-}$ production in these cells and to explore the triggering mechanism of redox signaling in the regulation of vascular function. For example, the finding of a relatively early SOD-blockable increase in $O_2^{\bullet-}$ levels outside CAMs may suggest that outward $O_2^{\bullet-}$ production in the early stage of M_1-receptor activation triggers intracellular increases in $O_2^{\bullet-}$ because addition of cell membrane-impermeable SOD outside cells blocked increases in

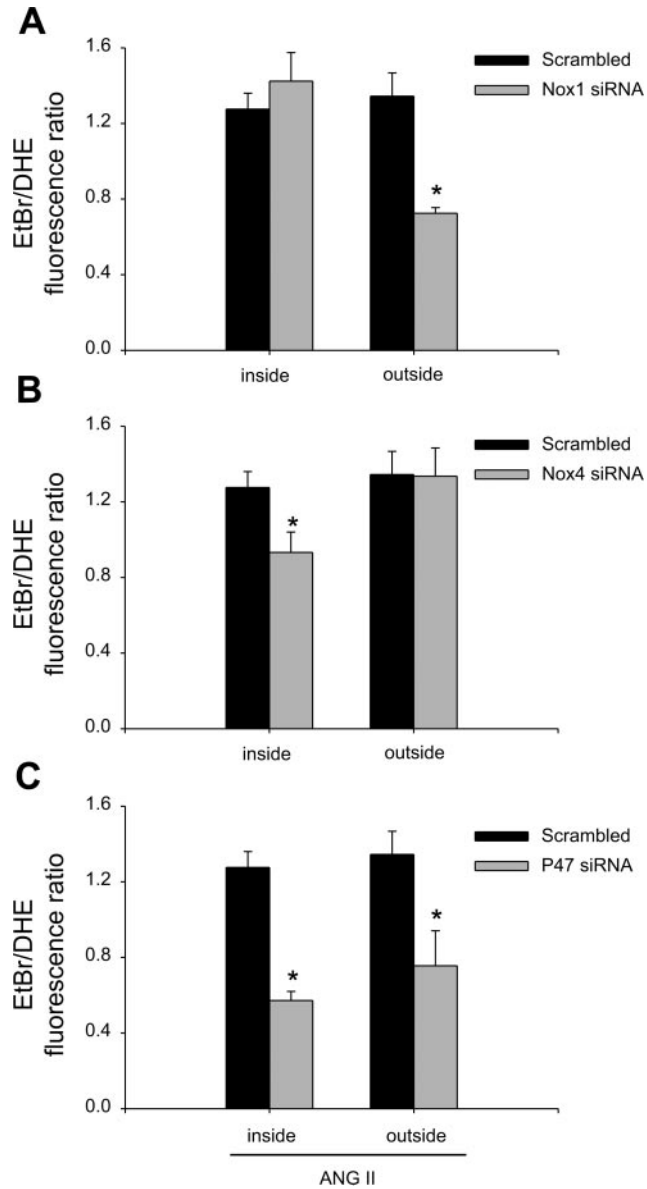

Fig. 9. Effects of RNA interference of NAD(P)H oxidase on ANG II-induced $O_2^{\bullet-}$ production inside and outside CAMs as measured by fluorescent microscopic imaging analysis. *A*: effect of Nox1 siRNA or scrambled, small RNA ($n = 6$ cases). *B*: effect of Nox4 siRNA or scrambled, small RNA ($n = 6$ cases). *C*: effect of $p47^{phox}$ siRNA or scrambled, small RNA ($n = 6$ cases). *$P < 0.05$ compared with values obtained from CAMs treated with scrambled, small RNA.

$O_2^{\bullet-}$ signals both outside and inside CAMs. In this regard, $O_2^{\bullet-}$ may serve as an autocrine to activate some membrane receptors or different signaling pathways to result in $O_2^{\bullet-}$ production from intracellular sources (45). In addition, $O_2^{\bullet-}$ can also enter the cells through its channels or other membrane carriers and activate intracellular $O_2^{\bullet-}$ production through different enzymes such as NAD(P)H oxidase. Recent studies have already demonstrated that NAD(P)H oxidase could be activated by $O_2^{\bullet-}$, leading to a positive feedback response (31). In the present study, we also tested whether extracellular $O_2^{\bullet-}$ stimulates NAD(P)H oxidase activation. It was found that addition of X/XO in the bath solution significantly induced extracellular and intracellular $O_2^{\bullet-}$ production with a pattern similar to that of OXO, which was markedly attenuated by NAD(P)H oxidase inhibitors. This indicates that $O_2^{\bullet-}$ from X/XO outside these cells at least partially exerts its action through enhanced intracellular $O_2^{\bullet-}$ production. This stimulatory action of $O_2^{\bullet-}$ on intracellular NAD(P)H oxidase may explain previous findings from our laboratory and by others that extracellular addition of the $O_2^{\bullet-}$-producing system largely increased intracellular $O_2^{\bullet-}$ (38, 58). Given the ionic characteristics of $O_2^{\bullet-}$, the entry of $O_2^{\bullet-}$ into cells should be relatively difficult. Therefore, increased intracellular $O_2^{\bullet-}$ under this condition would be primarily produced from activation of intracellular NAD(P)H oxidase. In addition, this redox activation of NAD(P)H oxidase by another ROS, H_2O_2, has also been reported recently (31).

There was a concern that the temporal difference between increased $O_2^{\bullet-}$ induced by M_1 agonist inside and outside cells may be due to different trapping or trafficking efficiency of intra- or extracellular $O_2^{\bullet-}$, since the DHE-oxidizing product ethidium needs to bind to DNA. However, some of our results demonstrated that this is not the case. First, we used another indicator, H_2DCFDA, which directly detects $O_2^{\bullet-}$ metabolite via SOD (H_2O_2) in cytoplasma and found a pattern of changes in intracellular and extracellular redox signals similar to what was observed with DHE as the indicator inside and outside CAMs. Second, when another agonist (ANG II) was used, a parallel increase in $O_2^{\bullet-}$ inside and outside these cells was observed. This is different from the pattern exhibited during M_1-receptor activation. These results further confirm that the spatiotemporal patterns of $O_2^{\bullet-}$ production observed by this monitoring system represent different responses of intracellular and extracellular production, rather than the artifact of the assays.

One of the major goals in the present study is to illustrate the production of $O_2^{\bullet-}$ outside CAMs because there is no direct evidence showing that vascular myocytes could produce $O_2^{\bullet-}$ toward the outside of these cells, despite this orientation of $O_2^{\bullet-}$ production being assumed (4, 25). In addition to fluorescent imaging analysis, the present study used three other different methods to demonstrate that CAMs could enzymatically produce $O_2^{\bullet-}$ toward the outside of these cells. These methods included microscopic detection of NBT staining, confocal microscopy analysis of extracellularly trapped H_2O_2 by Matrigel, and ESR measurements. It was found that M_1 agonist OXO induced formation of insoluble formazin-NBT precipitation on the surface of CAMs. This dye was widely used to determine activation of NAD(P)H oxidase in phagocytes for $O_2^{\bullet-}$ production during respiratory burst (39). Using confocal microscopy, we observed an increase in green fluorescence of OxyBURST H_2HFF BSA dye around CAMs in response to OXO, which indicates extracellular H_2O_2 increase (8). Because this BSA conjugate cannot enter cells, this detected green fluorescence represents extracellular ROS. Although this assay did not directly detect $O_2^{\bullet-}$ levels, the increase in H_2O_2 amount outside these cells under this short-term OXO stimulation is undoubtedly indicative of $O_2^{\bullet-}$ production or accumulation, since there is evidence that inhibition of NAD(P)H oxidase could attenuate the enhancement of this extracellular fluorescence derived from the BSA-H_2HFF conjugates. Finally, we performed ESR spectrometry to further confirm OXO-induced $O_2^{\bullet-}$ production outside these CAMs. In these experiments, SOD-sensitive components of ESR spectrometric signals in cell suspensions were analyzed to represent extracellular $O_2^{\bullet-}$. Given the high specificity of ESR trapping assay in detecting $O_2^{\bullet-}$, these experiments attempted to confirm that $O_2^{\bullet-}$ is detectable outside CAMS when they are stimulated by agonists. Although this ESR spectrometric assay could not use a single cell to detect $O_2^{\bullet-}$ level (9), it is important that the signal highly specific to $O_2^{\bullet-}$ can be detected outside CAMs, which can further support the view that an outward production of $O_2^{\bullet-}$ occurs in these cells in response to M_1-receptor activation. The results showed that the SOD-sensitive ESR signal was significantly increased when CAMs were stimulated by OXO. Taken together, all four different assays that we used in the present study consistently demonstrated that there is a mechanism by which $O_2^{\bullet-}$ is produced toward the outside of CAMs when their M_1 receptors are activated. This outwardly produced $O_2^{\bullet-}$ may play an autocrine or paracrine role in the regulation of vascular function.

To determine the contribution of NAD(P)H oxidase to increased extra- and intracellular $O_2^{\bullet-}$ production, we first examined the effects of two widely used NAD(P)H oxidase inhibitors (DPI and apocynin) on $O_2^{\bullet-}$ increases induced by OXO. Fluorescent imaging analysis demonstrated that, in the presence of either DPI or apocynin, OXO-induced increases in $O_2^{\bullet-}$ levels both outside and inside CAMs were substantially blocked. In particular, increased intracellular $O_2^{\bullet-}$ under this condition was completely abolished. This suggests that both extra- and intracellular $O_2^{\bullet-}$ are associated with the activity of NAD(P)H oxidase. Next, we examined the effects of RNA interference by specific siRNA of different subunits of NAD(P)H oxidase. It was found that introduction of Nox1 or p47^{phox}-specific siRNA significantly attenuated OXO-induced increases in $O_2^{\bullet-}$ production both inside and outside CAMs. However, when these cells were transferred with Nox4 siRNA, only the intracellular increase in $O_2^{\bullet-}$ was reduced. This Nox4 RNA interference had no effect on increased production of extracellular $O_2^{\bullet-}$. These results provide evidence that both extracellular and intracellular $O_2^{\bullet-}$ production are associated with NAD(P)H oxidase activity and that different mechanisms or isoforms of NAD(P)H oxidase may mediate $O_2^{\bullet-}$ production inside or outside these arterial myocytes. It seems that Nox1 rather than Nox4 is primarily responsible for the production of extracellular $O_2^{\bullet-}$, since Nox4 siRNA and Nox2 could not block the increase in $O_2^{\bullet-}$ outside CAMs. Although the attenuation of intra- and extracellular increases in $O_2^{\bullet-}$ by Nox1 siRNA seems to indicate that this isoform of NAD(P)H oxidase contributes to the production of $O_2^{\bullet-}$ both outside and inside these cells, as discussed above, the increase in intracellular $O_2^{\bullet-}$ via Nox1 may not be directly toward the inside of

these cells. It is possible that, in CAMs, Nox1 is activated by stimulation of M_1 receptors and then $O_2^{\bullet-}$, as an autocrine or paracrine, may lead to activation of an intracellular NAD(P)H oxidase, which may be Nox4 because Nox2 siRNA had no effect on increases in intracellular $O_2^{\bullet-}$. Several previous reports have indicated that Nox4 is a primary isoform responsible for intracellular $O_2^{\bullet-}$ production (44, 52). In this regard, Nox1 has been shown to be enriched in the membrane fraction and Nox4 predominantly in the intracellular compartments of vascular myocytes (20, 52). It is known that Nox1 is membrane bound and uses intracellular NADPH or NADH as substrate to produce $O_2^{\bullet-}$. Although there is a possibility that an extracellular NAD(P)H oxidase may be present (37), detectable $O_2^{\bullet-}$ outside CAMs in our preparations is mainly from an enzyme located inside cells because extracellular addition of NADPH (10 mM) was not found to induce any changes in $O_2^{\bullet-}$ production both inside and outside these cells. There are many possible mechanisms by which extracellular $O_2^{\bullet-}$ may further activate intracellular NAD(P)H oxidase to produce intracellular $O_2^{\bullet-}$. For example, extracellular $O_2^{\bullet-}$ has been reported to activate PKC and thereby result in phosphorylation of $p47^{phox}$, thus activating intracellular NAD(P)H (4). In other studies, extracellular $O_2^{\bullet-}$ was found to alter the activity of cell membrane ion channels such as inhibition of K^+ channels or activation of Ca^{2+} channels and increase intracellular Ca^{2+} concentrations. Because NAD(P)H oxidase activity is Ca^{2+} sensitive, increased Ca^{2+} would activate NAD(P)H oxidase activity (1). In addition, extracellular $O_2^{\bullet-}$ could be converted into H_2O_2, which can easily enter the cells to directly or through some other pathway activate NAD(P)H oxidase, resulting in intracellular $O_2^{\bullet-}$ production (31).

Another important finding of the present study was that ANG II stimulates CAMs to produce $O_2^{\bullet-}$ outside and inside CAMs in parallel, which is different from that observed when these cells were stimulated by OXO. This parallel increase in extracellular and intracellular $O_2^{\bullet-}$ production in response to ANG II could be blocked or substantially attenuated by either SOD plus CAT or NAD(P)H oxidase inhibitors, suggesting that NAD(P)H oxidase is also responsible for the $O_2^{\bullet-}$ production both outside and inside these arterial myocytes during ANG II stimulation. It is unclear why ANG II increases extracellular and intracellular $O_2^{\bullet-}$ production in parallel, whereas OXO increases $O_2^{\bullet-}$ production earlier extracellularly than intracellularly. One possible mechanism may be associated with their postreceptor activating pathways. In this regard, ANG II has been demonstrated to activate NAD(P)H oxidase through phosphorylation of its subunits such as $p47^{phox}$ (28). Given no specificity of this phosphorylation process to cellular compartments, NAD(P)H oxidase could be activated no matter where this enzyme is primarily located, either on the cell membrane or in intracellular compartments such as the sarcoplasmic reticulum (52), lysosomes (8), and even cytosol (17). Therefore, a parallel increase in extracellular and intracellular $O_2^{\bullet-}$ could be observed when ANG II was added. However, the M_1 agonist OXO may activate NAD(P)H oxidase through changes in cell membrane electrical feature such as depolarization of membrane, rather than phosphorylation. NAD(P)H oxidase electrogenic activation has been reported in some other cells (11, 29). This membrane electrogenic activation may lead to a rapid production of $O_2^{\bullet-}$ toward the outside of cells followed by activation of intracellular NAD(P)H oxidase through the autocrine action of $O_2^{\bullet-}$ or its metabolites outside these cells. Taken together, our results suggest that membrane-bound and intracellular organelle NAD(P)H oxidases could be activated with a temporal difference when arterial myocytes receive different agonistic stimuli.

It should be noted that NAD(P)H oxidase activation may not require $p47^{phox}$ in some other cell types. For example, Martyn et al. (33) reported that this phox subunit is not needed for NAD(P)H oxidase activation in epithelial cell. We also found that, in renal mesangial cells, $p47^{phox}$ translocation from cytosol to membrane does not occur during different stimuli (50). However, this $p47^{phox}$ translocation is strongly required by bovine coronary endothelial cells (59). In VSMCs, considerable evidence shows that $p47^{phox}$ is needed during activation of NAD(P)H oxidase (24). Our results using $p47^{phox}$ siRNA demonstrate that both intracellular and extracellular $O_2^{\bullet-}$ productions require $p47^{phox}$.

In summary, the present study demonstrated the following. *1*) M_1-receptor activation stimulated $O_2^{\bullet-}$ production both outside and inside CAMs with a spatiotemporal pattern of more rapid extracellular increase in $O_2^{\bullet-}$ levels followed by a slow increase in intracellular $O_2^{\bullet-}$ levels. This $O_2^{\bullet-}$ production induced by M_1 agonist is due to NAD(P)H oxidase activation. *2*) Nox1 was found to primarily contribute to extracellular $O_2^{\bullet-}$ production, whereas Nox4 is a dominant enzyme responsible for intracellular $O_2^{\bullet-}$ generations. *3*) ANG II also stimulated both extra- and intracellular $O_2^{\bullet-}$ production, but the spatiotemporal pattern was different from that observed during M_1 agonist stimulation, which increases $O_2^{\bullet-}$ levels outside and inside CAMs in parallel. This difference of the spatiotemporal pattern of $O_2^{\bullet-}$ production in CAMs in response to different agonists may be related to different activating mechanism of NAD(P)H oxidase when these cells receive stimuli. It is concluded that, in response to different agonists, CAMs exhibit different spatiotemporal patterns of $O_2^{\bullet-}$ production, which is associated with NAD(P)H oxidase activation. Extracellular $O_2^{\bullet-}$ production through Nox1 on the cell membrane represents an autocrine or paracrine model by which $O_2^{\bullet-}$ may exert an important role in autocrine regulation or cell-cell communication in coronary arteries.

GRANTS

This study was supported by National Heart, Lung, and Blood Institute Grants HL-57244, HL-75316, and HL-70726.

REFERENCES

1. **Ameziane-El-Hassani R, Morand S, Boucher J-L, Frapart Y-M, Apostolou D, Agnandji D, Gnidehou S, Ohayon R, Noel-Hudson M-S, Francon J, Lalaoui K, Virion A, Dupuy C.** Dual oxidase-2 has an intrinsic Ca^{2+}-dependent H_2O_2-generating activity. *J Biol Chem* 280: 30046–30054, 2005.
2. **Becker LB, vanden Hoek TL, Shao ZH, Li CQ, Schumacker PT.** Generation of superoxide in cardiomyocytes during ischemia before reperfusion. *Am J Physiol Heart Circ Physiol* 277: H2240–H2246, 1999.
3. **Beckman J, Minor R Jr, White C, Repine J, Rosen G, Freeman B.** Superoxide dismutase and catalase conjugated to polyethylene glycol increases endothelial enzyme activity and oxidant resistance. *J Biol Chem* 263: 6884–6892, 1988.
4. **Brandes RP, Kreuzer J.** Vascular NADPH oxidases: molecular mechanisms of activation. *Cardiovasc Res* 65: 16–27, 2005.
5. **Cai H.** NAD(P)H oxidase-dependent self-propagation of hydrogen peroxide and vascular disease. *Circ Res* 96: 818–822, 2005.
6. **Carter WO, Narayanan PK, Robinson JP.** Intracellular hydrogen peroxide and superoxide anion detection in endothelial cells. *J Leukoc Biol* 55: 253–258, 1994.

7. **Chalupsky K, Cai H.** Endothelial dihydrofolate reductase: critical for nitric oxide bioavailability and role in angiotensin II uncoupling of endothelial nitric oxide synthase. *Proc Natl Acad Sci USA* 102: 9056–9061, 2005.
8. **Chen CS.** Phorbol ester induces elevated oxidative activity and alkalization in a subset of lysosomes. *BMC Cell Biol* 3: 21, 2002.
9. **Cherednichenko G, Zima AV, Feng W, Schaefer S, Blatter LA, Pessah IN.** NADH oxidase activity of rat cardiac sarcoplasmic reticulum regulates calcium-induced calcium release. *Circ Res* 94: 478–486, 2004.
10. **Cotter MA, Cameron NE.** Effect of the NAD(P)H oxidase inhibitor, apocynin, on peripheral nerve perfusion and function in diabetic rats. *Life Sci* 73: 1813–1824, 2003.
11. **DeCoursey TE, Morgan D, Cherny VV.** The voltage dependence of NADPH oxidase reveals why phagocytes need proton channels. *Nature* 422: 531–534, 2003.
12. **Di Wang H, Pagano PJ, Du Y, Cayatte AJ, Quinn MT, Brecher P, Cohen RA.** Superoxide anion from the adventitia of the rat thoracic aorta inactivates nitric oxide. *Circ Res* 82: 810–818, 1998.
13. **Garrett IR, Boyce BF, Oreffo RO, Bonewald L, Poser J, Mundy GR.** Oxygen-derived free radicals stimulate osteoclastic bone resorption in rodent bone in vitro and in vivo. *J Clin Invest* 85: 632–639, 1990.
14. **Ge ZD, Zhang DX, Chen YF, Yi FX, Zou AP, Campbell WB, Li PL.** Cyclic ADP-ribose contributes to contraction and Ca^{2+} release by M1 muscarinic receptor activation in coronary arterial smooth muscle. *J Vasc Res* 40: 28–36, 2003.
15. **Griendling KK, Minieri CA, Ollerenshaw JD, Alexander RW.** Angiotensin II stimulates NADH and NADPH oxidase activity in cultured vascular smooth muscle cells. *Circ Res* 74: 1141–1148, 1994.
16. **Griendling KK, Sorescu D, and Ushio-Fukai M.** NAD(P)H oxidase: role in cardiovascular biology and disease. *Circ Res* 86: 494–501, 2000.
17. **Gupte SA, Kaminski PM, Floyd B, Agarwal R, Ali N, Ahmad M, Edwards J, Wolin MS.** Cytosolic NADPH may regulate differences in basal Nox oxidase-derived superoxide generation in bovine coronary and pulmonary arteries. *Am J Physiol Heart Circ Physiol* 288: H13–H21, 2005.
18. **Hancock JT, Maly FE, Jones OT.** Properties of the superoxide-generating oxidase of B-lymphocyte cell lines. Determination of Michaelis parameters. *Biochem J* 262: 373–375, 1989.
19. **Heitzer T, Wenzel U, Hink U, Krollner D, Skatchkov M, Stahl RA, MacHarzina R, Brasen JH, Meinertz T, Munzel T.** Increased NAD(P)H oxidase-mediated superoxide production in renovascular hypertension: evidence for an involvement of protein kinase C. *Kidney Int* 55: 252–260, 1999.
20. **Hilenski LL, Clempus RE, Quinn MT, Lambeth JD, Griendling KK.** Distinct subcellular localizations of Nox1 and Nox4 in vascular smooth muscle cells. *Arterioscler Thromb Vasc Biol* 24: 677–683, 2004.
21. **Igarashi R, Hoshino J, Ochiai A, Morizawa Y, Mizushima Y.** Lecithinized superoxide dismutase enhances its pharmacologic potency by increasing its cell membrane affinity. *J Pharmacol Exp Ther* 271: 1672–1677, 1994.
22. **Jia L, Furchgott RF.** Inhibition by sulfhydryl compounds of vascular relaxation induced by nitric oxide and endothelium-derived relaxing factor. *J Pharmacol Exp Ther* 267: 371–378, 1993.
23. **Koedel U, Pfister HW.** Superoxide production by primary rat cerebral endothelial cells in response to pneumococci. *J Neuroimmunol* 96: 190–200, 1999.
24. **Landmesser U, Cai H, Dikalov S, McCann L, Hwang J, Jo H, Holland SM, Harrison DG.** Role of $p47^{phox}$ in vascular oxidative stress and hypertension caused by angiotensin II. *Hypertension* 40: 511–515, 2002.
25. **Lassegue B, Clempus RE.** Vascular NAD(P)H oxidases: specific features, expression, and regulation. *Am J Physiol Regul Integr Comp Physiol* 285: R277–R297, 2003.
26. **Laurindo FR, da Luz PL, Uint L, Rocha TF, Jaeger RG, Lopes EA.** Evidence for superoxide radical-dependent coronary vasospasm after angioplasty in intact dogs. *Circulation* 83: 1705–1715, 1991.
27. **Leung E, Johnston CI, Woodcock EA.** Stimulation of phosphatidylinositol metabolism in atrial and ventricular myocytes. *Life Sci* 39: 2215–2220, 1986.
28. **Li JM, Shah AM.** Mechanism of endothelial cell NADPH oxidase activation by angiotensin II. Role of the $p47^{phox}$ subunit. *J Biol Chem* 278: 12094–12100, 2003.
29. **Li N, Zhang G, Yi FX, Zou AP, Li PL.** Activation of NAD(P)H oxidase by outward movements of H+ ions in renal medullary thick ascending limb of Henle. *Am J Physiol Renal Physiol* 289: F1048–F1056, 2005.
30. **Li VX, Lee TT, Siebenaler JF, Rusch NJ, Li PL.** Characterization of NAD(P)H oxidase-associated electron currents across plasma membranes of coronary vascular smooth muscle cells. *FASEB J* 19: 630–637, 2005.
31. **Li WG, Miller FJ Jr, Zhang HJ, Spitz DR, Oberley LW, Weintraub NL.** H_2O_2-induced O_2 production by a non-phagocytic NAD(P)H oxidase causes oxidant injury. *J Biol Chem* 276: 29251–29256, 2001.
32. **Liu JQ, Folz RJ.** Extracellular superoxide enhances 5-HT-induced murine pulmonary artery vasoconstriction. *Am J Physiol Lung Cell Mol Physiol* 287: L111–L118, 2004.
33. **Martyn KD, Frederick LM, von Loehneysen K, Dinauer MC, Knaus UG.** Functional analysis of Nox4 reveals unique characteristics compared to other NADPH oxidases. *Cell Signal* 18: 69–82, 2006.
34. **Matsunaga K, Furchgott RF.** Responses of rabbit aorta to nitric oxide and superoxide generated by ultraviolet irradiation of solutions containing inorganic nitrite. *J Pharmacol Exp Ther* 259: 1140–1146, 1991.
35. **Mohazzab KM, Kaminski PM, Wolin MS.** NADH oxidoreductase is a major source of superoxide anion in bovine coronary artery endothelium. *Am J Physiol Heart Circ Physiol* 266: H2568–H2572, 1994.
36. **Mori T, Cowley AW Jr.** Renal oxidative stress in medullary thick ascending limbs produced by elevated NaCl and glucose. *Hypertension* 43: 341–346, 2004.
37. **Morre DJ, Morre DM.** Cell surface NADH oxidases (ECTO-NOX proteins) with roles in cancer, cellular time-keeping, growth, aging and neurodegenerative diseases. *Free Radic Res* 37: 795–808, 2003.
38. **Paradies G, Petrosillo G, Pistolese M, Ruggiero FM.** Reactive oxygen species affect mitochondrial electron transport complex I activity through oxidative cardiolipin damage. *Gene* 286: 135–141, 2002.
39. **Schrenzel J, Serrander L, Banfi B, Nusse O, Fouyouzi R, Lew DP, Demaurex N, Krause K-H.** Electron currents generated by the human phagocyte NADPH oxidase. *Nature* 392: 734–737, 1998.
40. **Sorescu D, Weiss D, Lassegue B, Clempus RE, Szocs K, Sorescu GP, Valppu L, Quinn MT, Lambeth JD, Vega JD, Taylor WR, Griendling KK.** Superoxide production and expression of nox family proteins in human atherosclerosis. *Circulation* 105: 1429–1435, 2002.
41. **Teggatz EG, Zhang G, Zhang AY, Yi F, Li N, Zou AP, Li PL.** Role of cyclic ADP-ribose in Ca^{2+}-induced Ca^{2+} release and vasoconstriction in small renal arteries. *Microvasc Res* 70: 65–75, 2005.
42. **Wolfram Kuhlmann CR, Wiebke Ludders D, Schaefer CA, Kerstin Most A, Backenkohler U, Neumann T, Tillmanns H, Erdogan A.** Lysophosphatidylcholine-induced modulation of Ca^{2+}-activated K^+ channels contributes to ROS-dependent proliferation of cultured human endothelial cells. *J Mol Cell Cardiol* 36: 675–682, 2004.
43. **Wolin MS.** Reactive oxygen species and vascular signal transduction mechanisms. *Microcirculation* 3: 1–17, 1996.
44. **Wolin MS.** Subcellular localization of Nox-containing oxidases provides unique insight into their role in vascular oxidant signaling. *Arterioscler Thromb Vasc Biol* 24: 625–627, 2004.
45. **Wolin MS, Ahmad M, Gupte SA.** Oxidant and redox signaling in vascular oxygen sensing mechanisms: basic concepts, current controversies, and potential importance of cytosolic NADPH. *Am J Physiol Lung Cell Mol Physiol* 289: L159–L173, 2005.
46. **Wolin MS, Ahmad M, Gupte SA.** The sources of oxidative stress in the vessel wall. *Kidney Int* 67: 1659–1661, 2005.
47. **Wu DM, Kawamura H, Sakagami K, Kobayashi M, Puro DG.** Cholinergic regulation of pericyte-containing retinal microvessels. *Am J Physiol Heart Circ Physiol* 284: H2083–H2090, 2003.
48. **Yang ZZ, Zhang AY, Yi FX, Li PL, Zou AP.** Redox regulation of HIF-1α levels and HO-1 expression in renal medullary interstitial cells. *Am J Physiol Renal Physiol* 284: F1207–F1215, 2003.
49. **Yang ZZ, Zou AP.** Transcriptional regulation of heme oxygenases by HIF-1α in renal medullary interstitial cells. *Am J Physiol Renal Physiol* 281: F900–F908, 2001.

50. **Yi F, Zhang AY, Janscha JL, Li PL, Zou AP.** Homocysteine activates NADH//NADPH oxidase through ceramide-stimulated Rac GTPase activity in rat mesangial cells. *Kidney Int* 66: 1977–1987, 2004.
51. **Yi FX, Zhang AY, Campbell WB, Zou AP, van Breemen C, Li PL.** Simultaneous in situ monitoring of intracellular Ca2+ and NO in endothelium of coronary arteries. *Am J Physiol Heart Circ Physiol* 283: H2725–H2732, 2002.
52. **Yi XY, Li VX, Zhang F, Yi F, Matson DR, Jiang MT, Li PL.** Characteristics and actions of NAD(P)H oxidase on the sarcoplasmic reticulum of coronary arterial smooth muscle. *Am J Physiol Heart Circ Physiol* 290: H1136–H1144, 2006.
53. **Yokoyama M, Inoue N, Kawashima S.** Role of the vascular NADH/NADPH oxidase system in atherosclerosis. *Ann NY Acad Sci* 902: 241–248, 2000.
54. **Zalba G, Jose GS, Moreno MU, Fortuno MA, Fortuno A, Beaumont FJ, Diez J.** Oxidative stress in arterial hypertension: role of NAD(P)H oxidase. *Hypertension* 38: 1395–1399, 2001.
55. **Zhang AY, Teggatz EG, Zou AP, Campbell WB, Li PL.** Endostatin uncouples NO and Ca^{2+} response to bradykinin through enhanced $O_2^{\bullet-}$ production in the intact coronary endothelium. *Am J Physiol Heart Circ Physiol* 288: H686–H694, 2005.
56. **Zhang AY, Yi F, Zhang G, Gulbins E, Li PL.** Lipid raft clustering and redox signaling platform formation in coronary arterial endothelial cells. *Hypertension* 47: 74–80, 2006.
57. **Zhang DX, Yi FX, Zou AP, Li PL.** Role of ceramide in TNF-α-induced impairment of endothelium-dependent vasorelaxation in coronary arteries. *Am J Physiol Heart Circ Physiol* 283: H1785–H1794, 2002.
58. **Zhang DX, Zou AP, Li PL.** Ceramide reduces endothelium-dependent vasodilation by increasing superoxide production in small bovine coronary arteries. *Circ Res* 88: 824–831, 2001.
59. **Zhang DX, Zou AP, Li PL.** Ceramide-induced activation of NADPH oxidase and endothelial dysfunction in small coronary arteries. *Am J Physiol Heart Circ Physiol* 284: H605–H612, 2003.